Perfluoropolyether Lubricant Depletion and Reflow in Hard Disk Drives

A THESIS
SUBMITTED TO THE FACULTY OF
UNIVERSITY OF MINNESOTA
BY

Paul Taylor

IN PARTIAL FULFILLMENT OF THE REQUIREMENTS
FOR THE DEGREE OF
MASTER OF ENGINEERING

Xiang Cheng

January 2017

Acknowledgements

I would first like to thank my advisor, Dr. Xiang Cheng, for his willingness to take on the role and for his guidance throughout my project. Additional thanks to the rest of my thesis committee, Dr. Kevin Dorfman and Dr. Jiarong Hong, for taking the time to review my thesis, provide feedback, and participate in my final examination. I would also like to thank my colleagues in the head-disk interface group who taught me the skills necessary to finish this project and supported me throughout. Finally, I would like to thank my family and friends, whose encouragement and support have made this work possible.

Abstract

In this study, the effects of on-track dwell time on a hard disk drive (HDD) multidentate perfluoropolyether media lubricant were investigated. It was found that increasing dwell times increase the magnitude of lubricant depletion to a point, after which the depletion does not increase with increasing dwell time. Light interference with the media and high skew angles were shown to increase depletion. Once the dwell is complete, it was found that the lubricant reflows into the depletion region. This reflow was shown to be accelerated by increasing humidity and temperature. The rates for both depletion and reflow were measured and used to develop a simple model. This model was used to predict the final depletion depth for a sample that experienced a sequence of on-/off- track dwell steps. Experimental verification of this model found that it is reasonably accurate, especially for short dwell times and long off-track reflow periods.

Table of Contents

List of Tables

List of Figures

1. Introduction

A recent white paper suggests that the demand for storage by the year 2020 will be 40,000 exabytes or 40 trillion gigabytes.[1] Much of this new data will be stored on hard disk drives and, in order to fit as much data as possible into each device or data center, future hard drives must continually increase the areal density of data stored on the media.[2]

A. Hard Drive Overview

A hard disk drive (Figure 1) consists of two principle components: rotating magnetic media and the slider that flies over it.[2] The head slider consists of an Al-Ti-C air bearing coated with a thin layer of diamond like carbon (DLC). The media consists of a glass or Al substrate coated with a Fe-Co magnetic layer, and a DLC overcoat and thin layer (0.8 – 1.4 nm[3]) of lubricant to protect the delicate magnetics.[2]

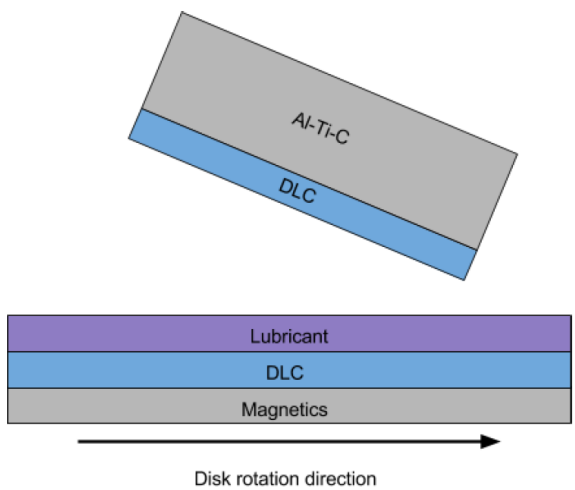

Figure 1: Schematic of head-disk interface; Magnetic layer, diamond like carbon coating, and lubricant shown on media; Diamond-like carbon and ceramic Al-Ti-C shown on slider.

To achieve higher data densities, the spacing between the read/write transducers and the magnetic media must be continually reduced.[2,4] This small separation places a significant tribological stress on the interface, which is already very harsh with spacing on the order of 1 – 2 nm, contact speeds of 10 – 40 m/s and shear rates of 10^{10} s^{-1}.[3] The

integrity of the media lubricant is of particular concern as the head disk spacing is reduced.

B. Media Lubricant

The typical hard drive lubricant is a low molecular weight (~2000 g/mol) perfluoropolyether with hydroxyl or amine end-groups to facilitate adhesion to the media.[3,5] . The lubricant is deposited on the media using either a dip coating process from a fluorinated solvent or using a vapor-phase deposition process and the resulting film is usually a monolayer or less in thickness (1 -2 nm).[3] Some examples of commercial lubricants include ZDol and Z-Tetraol, which respectively have one or two hydroxyl groups at each chain end. Most modern hard disk drives use a multidentate lubricant, such as ZTMD (Z-Tetraol Multidentate). ZTMD consists of coupled Z-Tetraol chains that result in multiple hydroxyl groups spaced along the length of the polymer chain which hold it close to the media, allowing for smaller head-disk spacings.[6] Typical structures are shown in Figure 2.[7]

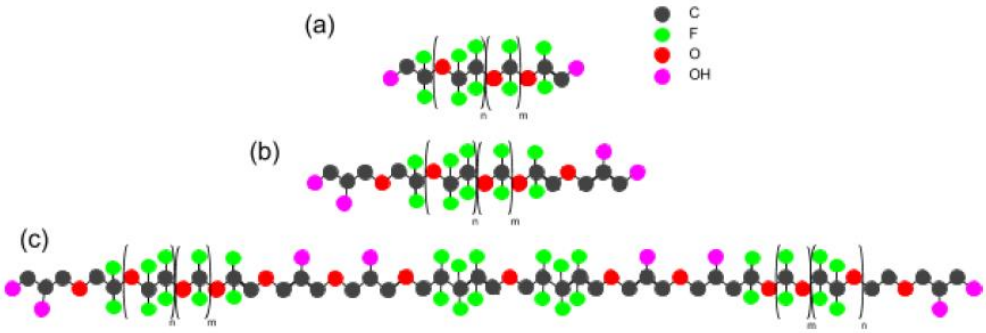

Figure 2: Lubricant molecular structures including: (a) Zdol (2 -OH), (b) Z-Tetraol (4 - OH), and Z-Tetraol Multidentate (ZTMD, 8 -OH)

C. Lubricant Depletion

One major lubricant-related issue is depletion (Figure 3). This can cause numerous issues in the drive including modulation[8] and transducer wear against the unlubricated disk[9]. Lubricant structure has been found to play a large role in the depletion. Specifically lubricants with multiple hydroxyl end-groups show significantly higher viscosity and are more difficult to deplete as a result.[10,11] The head/slider design also plays a role in

lubricant depletion, with larger center pad regions leading to larger amounts of lubricant depletion.[12]

In addition to structural effects, previous work has found that temperature and humidity play a role in lubricant flow. One study found that lubricant flow and the measured diffusivity increases slightly with increasing temperature.[13] A more significant factor in lubricant depletion is absolute humidity (in g / m^3), which was found in a separate study to have a strong positive correlation with depletion magnitude.[11] This effect was attributed to increased water molecule adsorption on the disk which creates competition for lubricant bonding sites.[14]

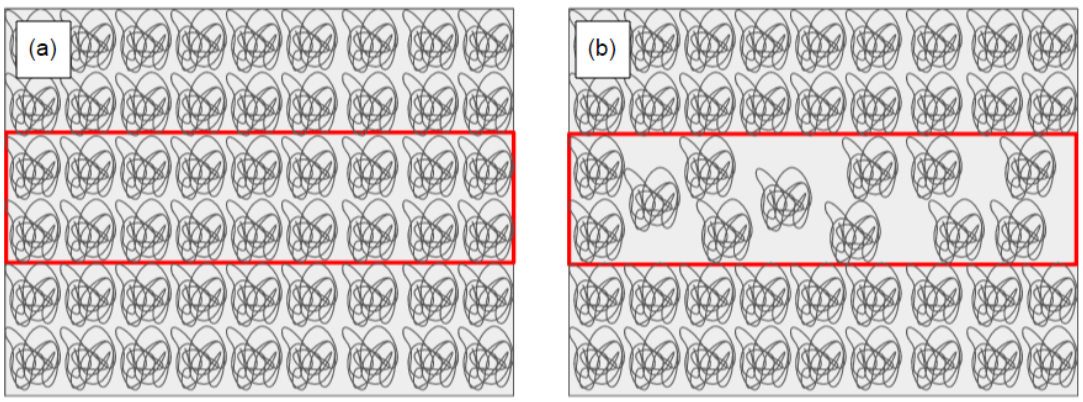

Figure 3: Schematic of lubricant distribution on a normal disk (a) and a disk with a depletion track (b). The measured depletion is a reduction in surface density or average thickness, not a reduction in thickness at every location.

D. Modeling Lubricant Flow

Lubricant spreading (ie reflow) is driven by an attractive potential between the liquid and the surface which is typically referred to as the disjoining pressure gradient (Equation 1).[15] The disjoining pressure typically consists of dispersive, electrostatic, and structural portions, but for very thin films we need only consider the dispersive interaction given in Equation 1.[16]

$$\Pi = \frac{A}{6\pi(h + d_0)^3}$$

Equation 1: Disjoining Pressure (Π), given by the Hamaker constant (A), film thickness (h), and distance of closest approach (d_0)

This pressure can be combined with the Navier-Stokes equation (lubrication approximation, no slip, and no stress at free surface) to give an expression for the differential thickness change (Equation 2). [15]

$$Q_{diffusion} = \frac{\delta h}{\delta t} = -\frac{\delta}{\delta x}\left[\left(\frac{h^3}{3\eta}\frac{d\Pi}{\delta h}\right)\frac{\delta h}{\delta x}\right]$$

Equation 2: Disjoining pressure (Π) driven flow given by the effective viscosity (η), the film thickness (h), and distance from depletion band (x)

Based on this equation one can define an effective diffusion coefficient (Equation 3)[15], which can be evaluated using an expression for the disjoining pressure in terms of the Hamaker constant[17] and an effective viscosity measured with lubricant blow-off experiments[18].

$$D = \left(\frac{h^3}{3\eta}\frac{d\Pi}{\delta h}\right) = \frac{Ah^3}{6\pi\eta(h+d_0)^4}$$

Equation 3: Effective diffusion coefficient (D) given by the effective viscosity (η), the Hamaker constant (A), the film thickness (h), and distance of closest approach (d_0)

Lubricant depletion due to the flying slider is a more complicated issue and multiple attempts have been made to model it accurately in the literature.[16,19–21] Depletion is difficult to model with molecular dynamics or direct simulation Monte Carlo due to the long length scales and the long time-scale of depletion events. In a recent study, the effects of shear stress, hydrodynamic pressure, and electrostatic pressure were considered and it was shown that the air shear stress is the dominant factor in lubricant displacement.[20] This air shear-driven flow is expressed by Dai et al as shown in Equation 4 .[20]

$$Q_{shear} = \frac{(h_0+h)^2\eta_a v}{2\eta(s_0+s-h)}$$

Equation 4: Air shear driven flow given by the effective viscosity (η), the air viscosity (η_a), the current and initial film thickness (h, h_0), the slider velocity (v), and the slider mean and modulating clearance (s_0, s)

Balancing the air shear and disjoining pressure driven flow gives the final expression (Equation 5) for the rate of lubricant depletion under a flying slider.[20]

$$\frac{\delta h}{\delta t} = Q_{shear} + Q_{diffusion} = \frac{(h_0 + h)^2 \eta_a v}{2\eta(s_0 + s - h)} - \frac{\delta}{\delta x}\left[\left(\frac{h^3}{3\eta}\frac{d\Pi}{\delta h}\right)\frac{\delta h}{\delta x}\right]$$

Equation 5: Differential height change based on shear/diffusion driven flow models

2. Experimental

A. Materials

All experiments were performed on 10K RPM hard disk drives. The media (disks) in this experiment were all standard 65 mm hard drive disks, with a glass substrate, cobalt magnetic layer, 2 - 4 nm amorphous carbon coating, and 1 - 2 nm lubricant layer. Lubricant structure is a proprietary multidentate lubricant. The heads in this experiment were standard 3 pad air bearing designs with an amorphous carbon coating.

B. Depletion Dwell Test Protocol

Lubricant depletion bands were generated by using the HDD servo system to seek to a specific track and dwell on that track (or combination of tracks) for an extended period of time (Figure 4). During that dwell step, the transducer region of the head was protruded using thermal actuators to contact the surface of the disk.[22,23] The amount of power required to reach this point was determined using standard contact detection techniques.[24] In most experiments the internal temperature was held constant at 35 C using an Espec environmental chamber, although in one experiment both temperature and humidity were varied using the chamber.

C. Depletion Measurements and Instrumentation

After testing, the disks were removed from the drives and lubricant depletion was measured (Figure 5) using a Candela 5100 Optical Surface Analyzer (OSA). This instrument uses a laser to measure phase shift as the polarized light is reflected off the surface of the disk.[8] The amount of phase shift is correlated with lubricant thickness, so with calibration this instrument can be used to give quantitative measurements of lubricant depletion.

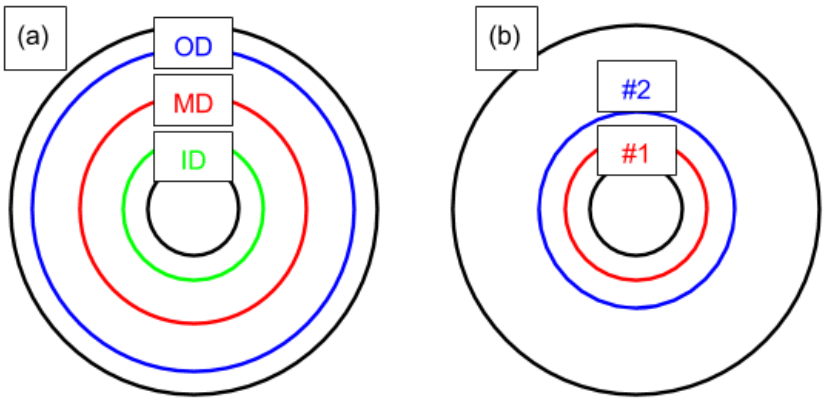

Figure 4: Schematic of dwell sequence. In (a) the head sits on one track for the duration of the test at either the outer, middle, or inner diameter (OD, MD, ID) of the disk. In (b) the head alternates between two tracks for the duration of the test.

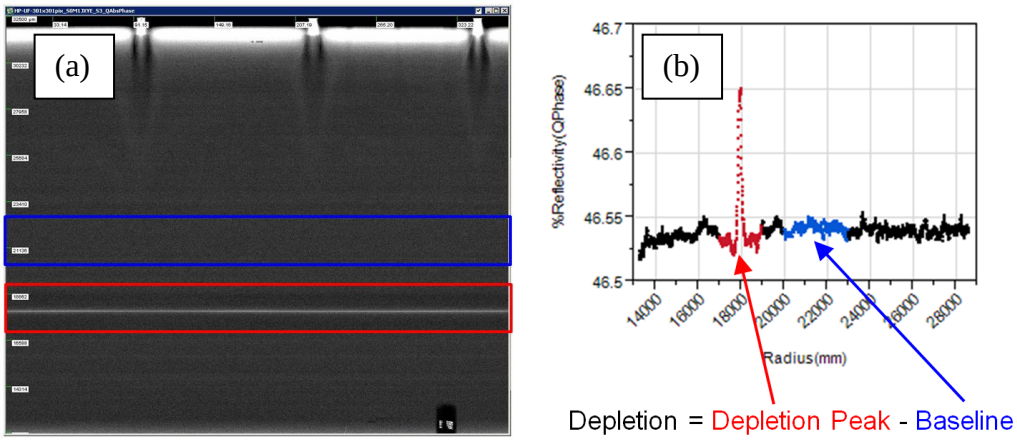

Figure 5: Depletion measurement technique. (a) shows sample Candela scan which is averaged around the circumference of the disk to give the plot shown in (b). (b) can then be used to calculate the depletion by subtracting the averaged baseline from the maximum of the depletion peak.

The OSA instrument was calibrated using a set of half-lubed calibration disks (Figure 6). These disks represent a ladder of thicknesses (measured using Fourier Transform Infrared Spectroscopy (FTIR)[25]) and the resulting signal can be used to create a calibration curve (Figure 7). This calibration curve can then be used on scans of disks with depletion bands to convert the change in reflectivity to a change in thickness (angstroms).

In order to measure reflow, the tested disks were allowed to sit at ambient temperature and humidity and the Candela measurements were repeated periodically to generate a curve of decreasing depletion vs time (Figure 8).

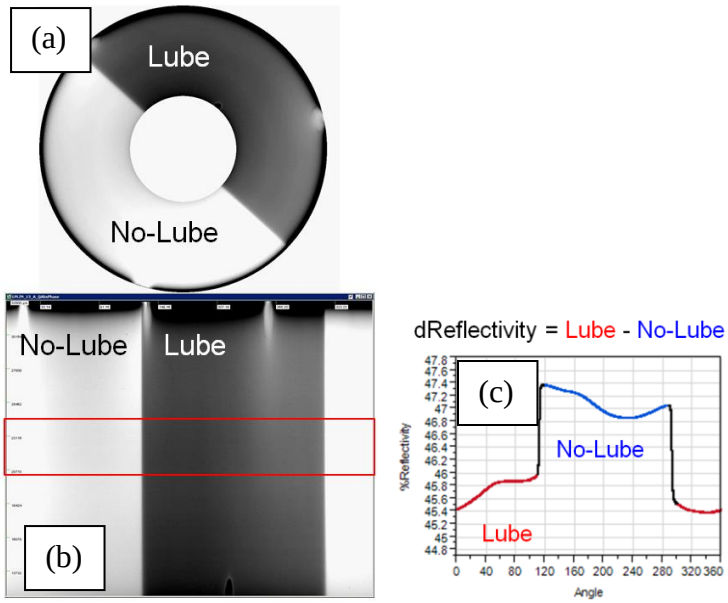

Figure 6: Optical surface analyzer calibration procedure. Images (a) and (b) depict polar and rectangular views of the disk from Candela. The plot (c) shows the track average through the box in (b) and can be used to calculate the change in reflectivity due to the lubricant by subtracting the average reflectivity in the lubed area from the un-lubed area.

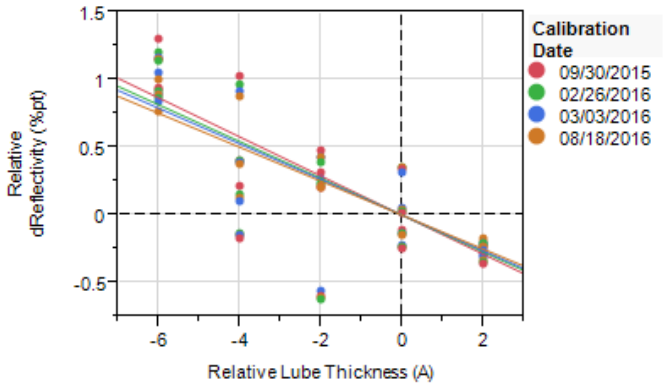

Figure 7: Calibration curve based on delta reflectivity numbers calculated from OSA measurements on calibration disks

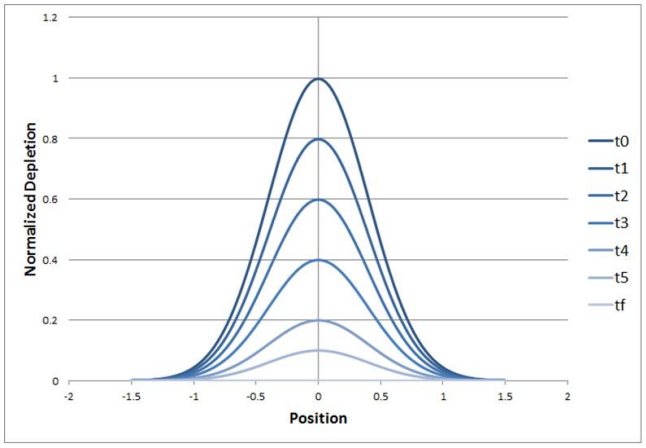

Figure 8: Schematic of reflow of depletion profile as a function of time

3. Results and Discussion

This study can be divided into three main sections. In the first section, the qualitative factors that influence lubricant depletion & reflow were investigated. These factors include time, temperature, clearance, and skew angle. In the second section, the results of the depletion/reflow vs time experiments were used to generate a model to predict depletion based on seek workload (time on/off track). In the third section the model was validated by dwelling with various workloads and comparing measured depletion with model predictions.

A. Lubricant Depletion and Reflow as a Function of Time

In the first experiment, the total on-track dwell time was varied from 1 - 30 h. After dwelling, the depletion was measured immediately and the measurement was repeated periodically for several days thereafter to measure the reflow of the depletion track. These data points were plotted to show the trend of depletion and reflow as a function of time (Figure 9).

As expected depletion increases as dwell time increases and tapers off after some critical point. This is reasonable because the diffusion coefficient is dependent on the thickness and, as a result, reflow will eventually equilibrate with the depletion.[19] Based on this result, a 3 h dwell was selected for future experiments because it occurs at a point of high sensitivity (both higher and lower depletion can easily occur).

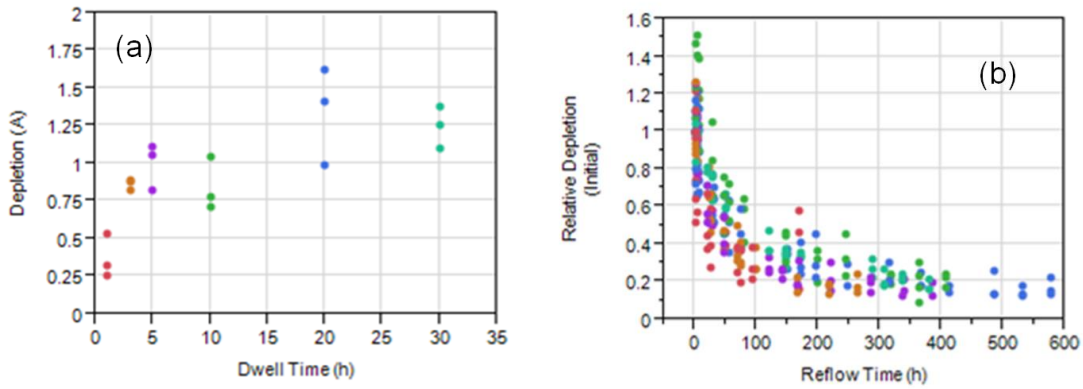

Figure 9: Depletion (a) and normalized reflow (b) as a function of time. Colored points correspond to different nominal dwell times.

The reflow profiles (Figure 10) show that depletion bands disappear over time, and that the rate of reflow is proportional to the initial depletion depth. This result is as-expected based on the thickness-dependent diffusion constant described in previous literature.[15] When the reflow profiles were normalized to the initial measurement, the curves overlap well (Figure 9). This suggests that the reflow profile has a strong dependence on the initial depletion level.

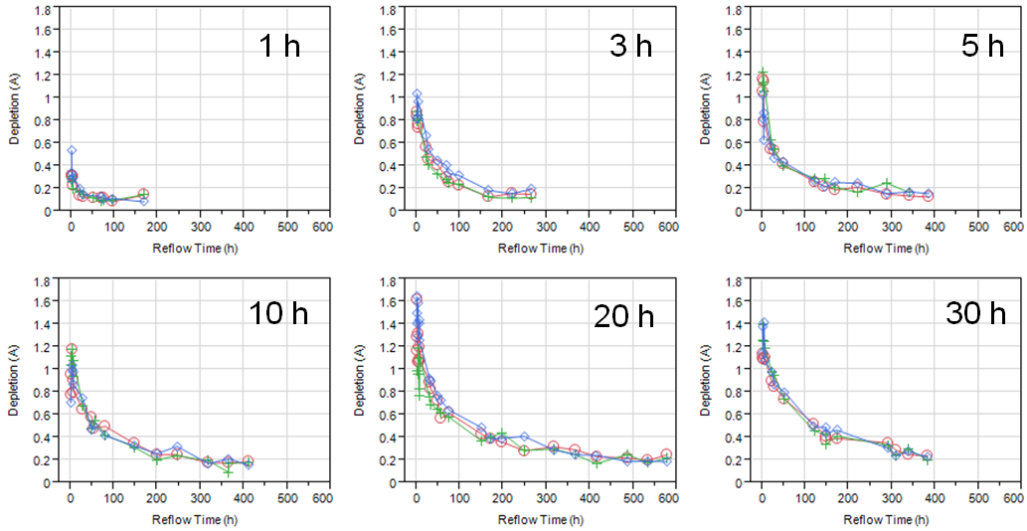

Figure 10: Reflow as a function of wait time and initial depletion (determined by dwell time shown in upper corner)

In addition to measuring the magnitude of the depletion, the width of the depletion was measured by fitting a Gaussian curve to the distribution (Figure 11) and calculating the

full width at half maximum (FWHM). This measurement was repeated at each reflow point for the depletion and reflow data vs time. This data set shows (Figure 12) that, in addition to decreasing in depth, the depletion bands also broaden as reflow occurs. The results also show that initial depletion width (100 - 200 um) is close to the total width of the pressurized region of the HDD transducer (~100 um)[12], a good confirmation that the head pressure is causing the lubricant to deplete.

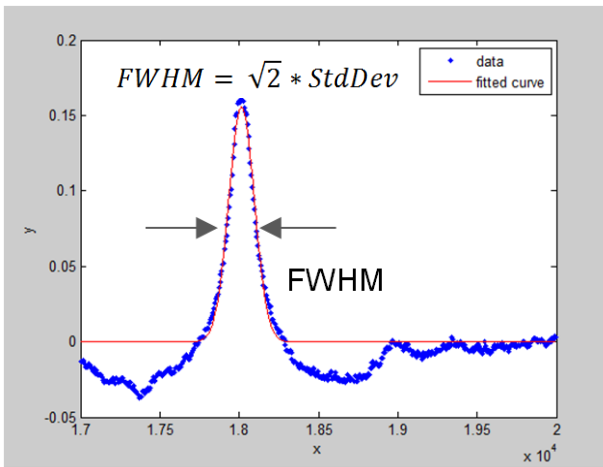

Figure 11: Measurement of depletion width using Gaussian fit

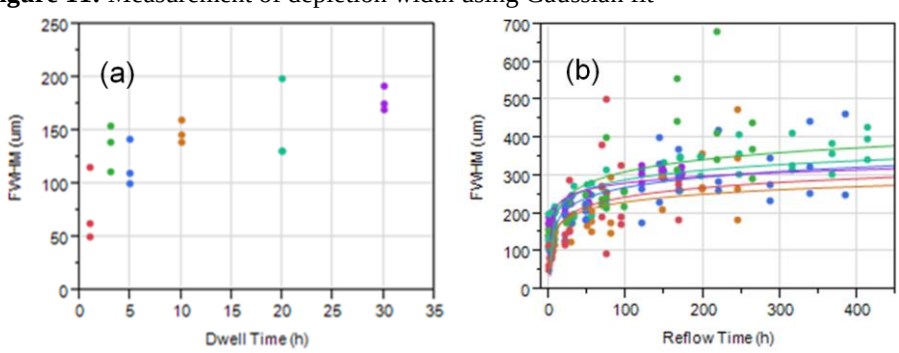

Figure 12: Plots of depletion width as a function of on-track dwell time (a) and post-test reflow time (b)

B. Skew Angle and Clearance Effects

The next goal was to determine how to optimize the dwell to maximize depletion signal and consistency. To this end, skew angle or (equivalently) dwell radius and active clearance (transducer protrusion) were varied to find the maximum depletion. The results (Figure 13) show that running the head at either the OD (outer diameter) or ID (inner diameter) of the disk result in the highest levels of depletion. Pressure under the slider is

highest at the OD of the disk[26], which may explain why the depletion is larger at that angle.

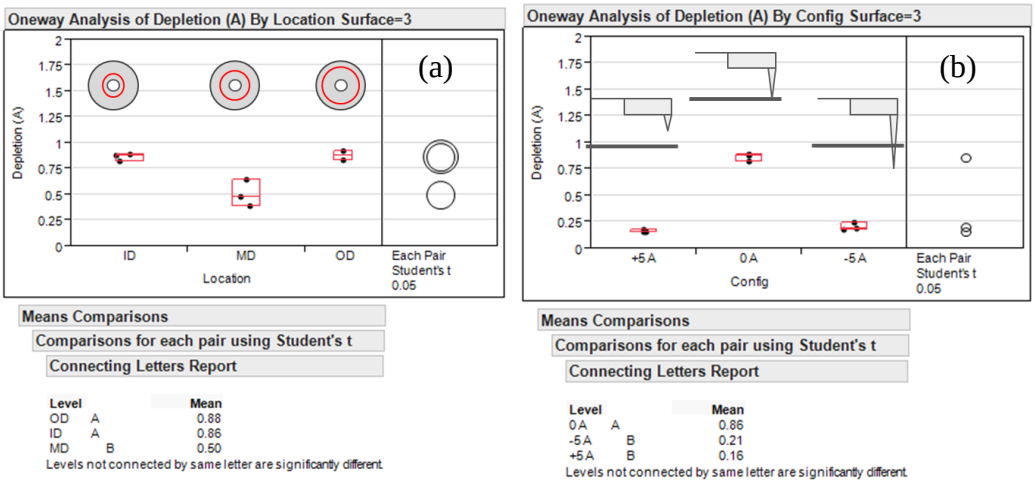

Figure 13: Depletion by dwell location (a) and active clearance (b). Most depletion at OD/ID and at 0A clearance (head is in light contact with disk)

The results also show that dwelling with the head in light contact with the disk (0 A clearance) caused more depletion than dwelling at a clearance slightly above the disk (+5 A) or pushing the head into the disk (-5 A). This may be due to increased modulation of the head when it is in light interference as compared with no interference or heavy interference. This "light contact" or "lube surfing" state has been shown in other experiments to cause lubricant depletion.[27]

As a result of this data, all later experiments were run at ID and 0 A clearance, due to ease of measurement and large response.

C. Temperature and Humidity Effects

Previous work[11,13] has shown that both temperature and humidity have an effect on lubricant diffusivity and reflow rates. An experiment was run to verify these results in the lubricant structure used in this study. As expected, it was found (Figure 14) that allowing the media to sit at high temperature/humidity conditions after depletion drastically increased the reflow rate. In contrast, increasing temperature and humidity did not seem to have a significant effect on depletion magnitude. This asymmetry is likely a result of

the fact that increasing diffusivity will increase both depletion and reflow so the net effect is not obvious.

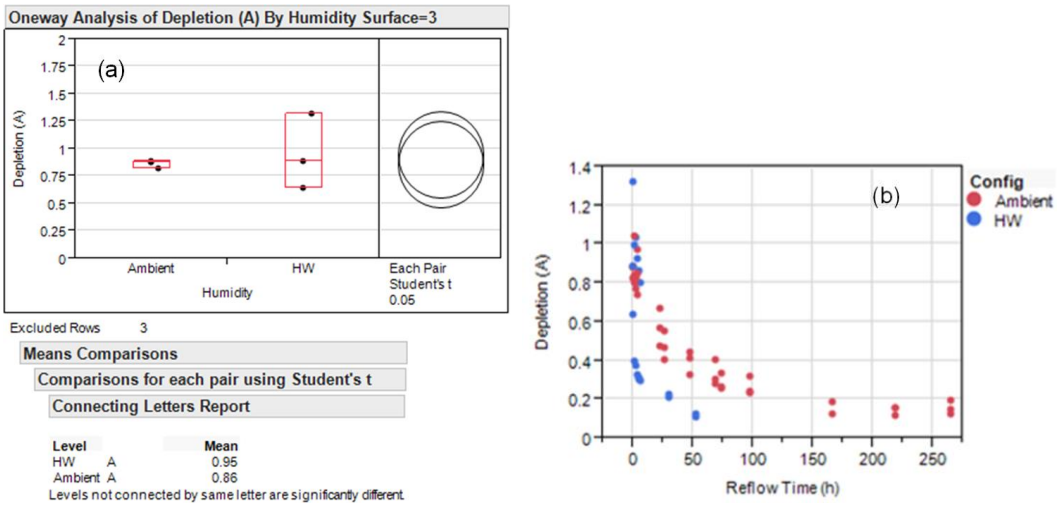

Figure 14: Depletion (a) and reflow (b) measured at ambient (25 C, 30% RH) and hot/wet (HW, 60 C, 80%RH) conditions

D. Depletion Modeling

Using the results of the depletion and reflow as a function time experiment, a simple model was developed from regressions to the data. The model alternates between increasing depletion using the depletion regression, and then decreasing depletion using the reflow model to simulate the final depletion level expected from an alternating workload. This analysis is shown schematically in Figure 15.

The reflow steps were modeled with a linear fit to the initial normalized data (Figure 16). The normalized data set was used due to the dependence of the reflow rate on film thickness, even in the case of a thickness independent diffusion constant as shown in Equation 6.[28] The linear fit is justified due to the relatively short modeled reflow timescales (seconds) as compared with the long reflow measurement timescales (hours) and the small amount of displaced lubricant (<10% of total thickness).

$$\frac{h(x,t)}{h^*} = \frac{\delta}{\sqrt{4Dt}} e^{-\frac{x^2}{4Dt}}$$

Equation 6: Diffusion into a depletion of finite width. Here h, h* are current and initial depletion depths, δ is the initial depletion width, D is the diffusion constant, x is the radial coordinate, and t is the elapsed time

As was previously discussed, the depletion process is more complicated than the reflow process due to the shear and pickup effects from the flying slider, and is difficult to model as a result. To craft our simple model, an expedient equation was chosen to fit the data (Figure 16). This expression passes through (0,0), increases rapidly and saturates at some finite depletion level, as observed in the experimental depletion data. It was assumed that the depletion will follow the same curve on each dwell cycle (Figure 15), without hysteresis. This assumption is reasonable because the balance between the shear induced flow out of the depletion band and the diffusion induced flow into the depletion band will be constant for a given depletion depth and will therefore give the same depletion rate.

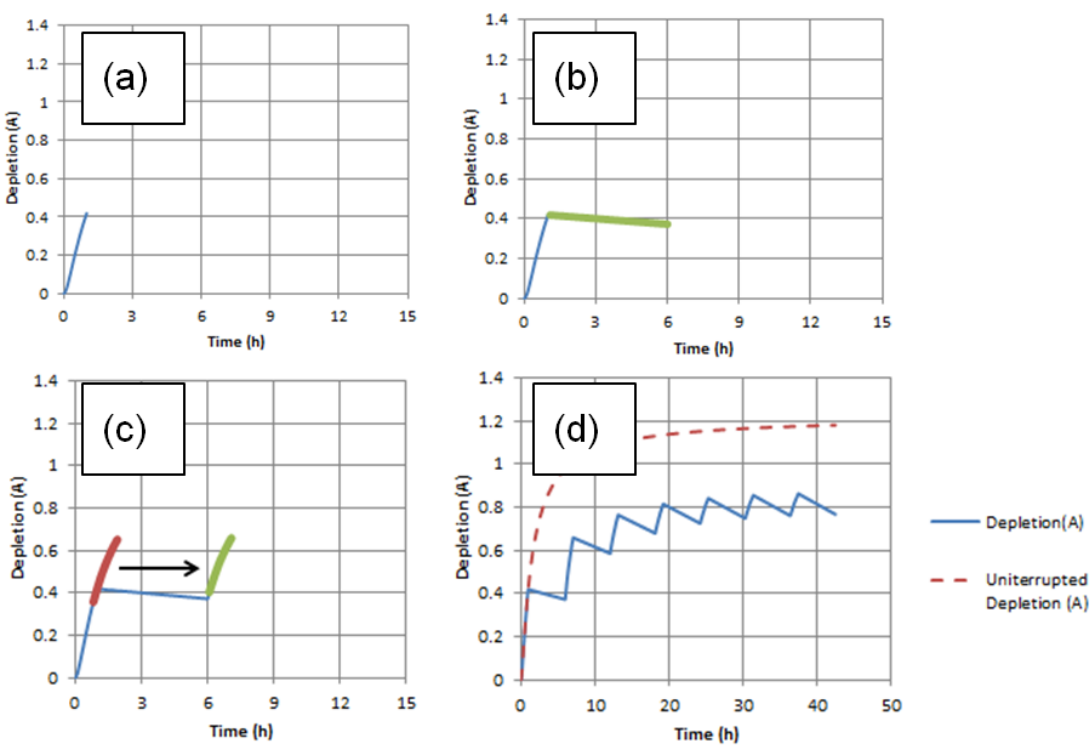

Figure 15: Model of depletion as a series of depletion and reflow events. (a) Start by increasing depletion for dwell time (blue). (b) Next reduce depletion by reflow rate for off-track time (green). (c) Then continue

on same depletion trajectory, offset in time (green). (d) Iterate this procedure to find where depletion saturates

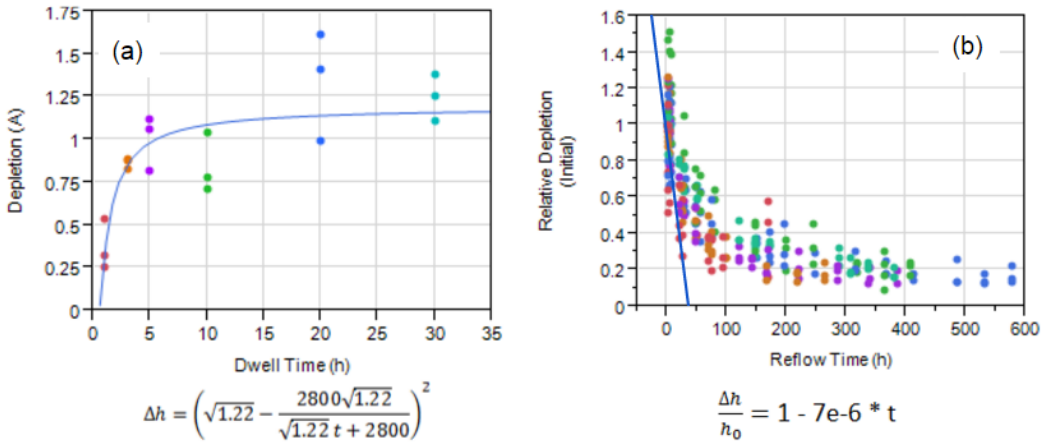

$$\Delta h = \left(\sqrt{1.22} - \frac{2800\sqrt{1.22}}{\sqrt{1.22}\,t + 2800}\right)^2 \qquad \frac{\Delta h}{h_0} = 1 - 7e\text{-}6 * t$$

Figure 16: Depletion (a) and reflow (b) regressions used for model. Here h is lube thickness and t is time in seconds. Reflow data shown is from measurements on spinning drives.

The results of the depletion-reflow model are shown in Figure 17. As can be seen from this plot, the model predicts that depletion depth will be reduced significantly as a larger fraction of test time is spent off of the depletion track. Additionally, the model shows that even spending 50% of time off of the depletion band allows enough reflow to significantly reduce the depletion depth.

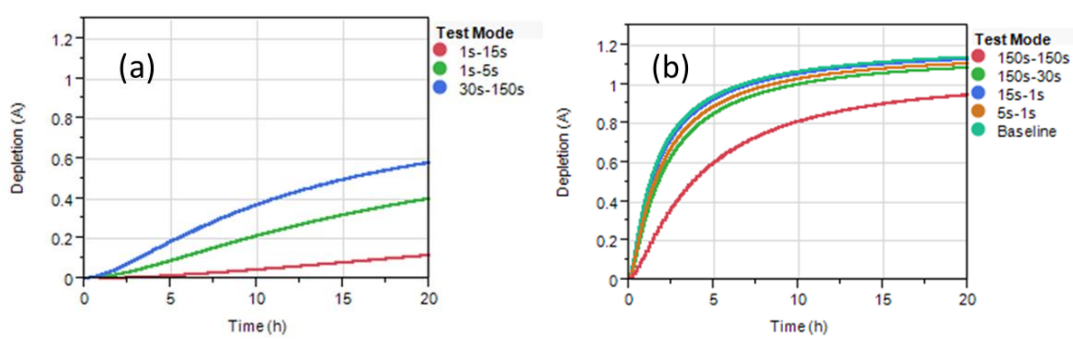

Figure 17: Modeled results for short (a) and long (b) on-track dwell times

E. Model Validation

In order to validate the model developed in the previous section, experiments were run in which the on- / off- track workload was varied as shown in Table 1 and the resulting depletion was compared with the predictions from the model. In all cases the entire

workload was repeated many times to give a total on-track time of ~20 h, which should be enough to saturate the depletion based on the depletion vs time experiments. The results of this experiment (Figure 18) show that, as expected, increasing the percentage of time on track increases depletion. In addition, it was found that even a small percentage of off-track time decreases depletion from the 100% on-track test. In addition, the limited results for short dwell times (long off-track times) match well with the results predicted by the depletion/reflow model (Figure 18).

Table 1: Experimental conditions for various workloads

On-Track (s)	Off-Track (s)	Total Time On-Track (h)	Percent On-Track
15	1	20	94%
5	1	20	83%
150	30	20	83%
1	5	20	17%
30	150	20	17%
1	15	20	6.25%

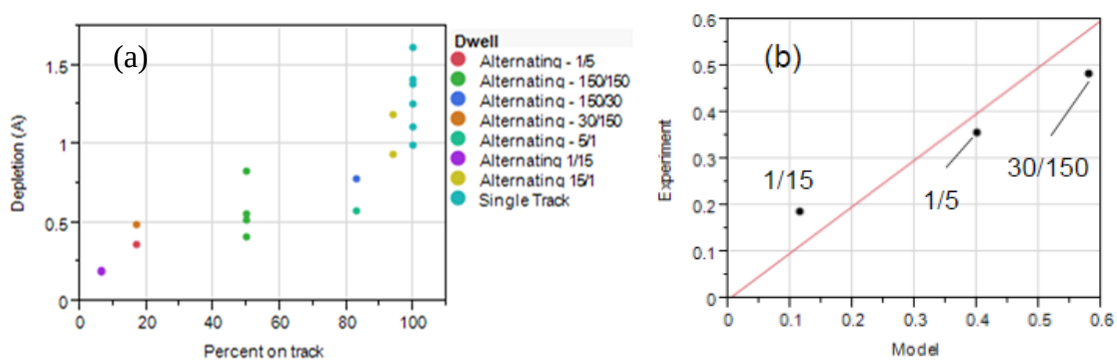

Figure 18: Depletion as a function of percent of time spent on track for various workloads (a) and comparison between experimental and modeled depletion for short on-track dwell times (b)

4. Conclusion

This study examined the factors that impact lubricant depletion in HDD media and attempted to create a model to predict depletion based on seek patterns and workloads. As expected, it was found that depletion increases with dwell time, but saturates due to an increasing reflow rate. Other factors, such as active clearance, skew angle, and absolute

humidity were found to have a significant effect on lubricant depletion. The simple model developed based on the reflow and depletion experiments proved effective in calculating the final depletion for a variety of on-/off- track dwell patterns and was validated by testing at those conditions.

The next steps for this line of inquiry would be to add humidity and temperature effects to the depletion model. In addition, an investigation into the effects of modulation and skew angle on lubricant depletion may be beneficial to improve the understanding of this phenomenon.

5. Bibliography

1. Gantz, J. & Reinsel, D. The digital universe in 2020: Big data, bigger digital shadows, and biggest growth in the far east. *IDC IView IDC Anal. Future* **2007,** 1–16 (2012).
2. Wood, R. Future hard disk drive systems. *J. Magn. Magn. Mater.* **321,** 555–561 (2009).
3. Bruno Marchon. Thin-film media lubricants: Structure, characterization, and performance. *Developments in Data Storage: Materials Perspective* 144 (2011).
4. Bruno Marchon & Terry Olson. Magnetic Spacing Trends: From LMR to PMR and Beyond. *IEEE Trans. Magn.* **45,** 3608–3611 (2009).
5. T.E. Karis, B. Marchon, D.A. Hopper & R.L. Siemens. Perfluoropolyether characterization by nuclear magnetic resonance spectroscopy and gel permeation chromatography. *J. Fluor. Chem.* **118,** 81–94 (2002).
6. X.C. Guo *et al.* Multidentate functionalized lubricant for ultralow head/disk spacing in a disk drive. *J Appl Phys* **100,** (2006).
7. Mate, C. M. Spreading Kinetics of Lubricant Droplets on Magnetic Recording Disks. *Tribol. Lett.* **51,** 385–395 (2013).
8. Remmelt Pit, Bruno Marchon, Steven Meeks & Vamsi Velidandla. Formation of lubricant 'moguls' at the head/disk interface. *Tribol. Lett.* **10,** 133–142 (2001).
9. Kim, S. H. *et al.* Durability Against Contact Wear of Nonlubricated Disks in the Head–Disk Interface of Disk Drives. *IEEE Trans. Magn.* **47,** 239–243 (2011).
10. X. Ma *et al.* Spreading of perfluoropolyalkylether films on amorphous carbon surfaces. *J. Chem. Phys.* **110,** 3129–3137 (1999).
11. Sang Hoon Kim, Qing Dai, Bruno Marchon & Karl Flechsig. Humidity effects on lubricant transfer in the head-disk interface of a hard disk drive. *J. Appl. Phys.* **105,** (2009).
12. Yijun Man, Bo Liu, Mingsheng Zhang & Leonard Gonzaga. Experimental study of slider–lubricant interaction with different slider designs. *Microsyst. Technol.* **15,** 1515–1520 (2009).
13. Xiaoding Ma, Huan Tang & Jing Gui. Temperature effect on spreading of perfluoropolyethers on amorphous carbon films. *Tribol. Lett.* **10,** 203–209 (2001).
14. Chen, H., Guo, Q., Li, L., Hsia, Y.-T. & Jhon, M. S. Humidity Effects on the Relaxation of Perfluoropolyether Lubricant Films. *IEEE Trans. Magn.* **42,** 2531–2533 (2006).
15. Marchon, B. & Karis, T. E. Poiseuille flow at a nanometer scale. *Europhys. Lett. EPL* **74,** 294–298 (2006).
16. Ono, K. Diffusion Equation for Spreading and Replenishment in Submonolayer Lubricant Film. *Tribol. Lett.* **57,** (2015).
17. Waltman, R. J., Tyndall, G. W. & Pacansky, J. Computer-Modeling Study of the Interactions of Zdol with Amorphous Carbon Surfaces. *Langmuir* **15,** 6470–6483 (1999).
18. Scarpulla, M. A., Mate, C. M. & Carter, M. D. Air shear driven flow of thin perfluoropolyether polymer films. *J. Chem. Phys.* **118,** 3368 (2003).

19. Saeki, F., Fukui, S. & Matsuoka, H. Analyses of Lubricant Deformation Caused by Gas Stresses and Surface Tension. *IEEE Trans. Magn.* **45,** 5061–5064 (2009).
20. Dai, Q., Hendriks, F. & Marchon, B. Modeling the washboard effect at the head/disk interface. *J. Appl. Phys.* **96,** 696 (2004).
21. Ma, X. *et al.* Complex terraced spreading of perfluoropolyalkylether films on carbon surfaces. *Phys. Rev. E* **59,** 722 (1999).
22. Masayuki Kurita *et al.* Active flying-height control slider using MEMS thermal actuator. *Microsyst. Technol.* **12,** 369–375 (2006).
23. M. Suk *et al.* Verification of thermally induced nanometer actuation of magnetic recording transducer to overcome mechanical and magnetic spacing challenges. *IEEE Trans. Magn.* **41,** 4350–4352 (2005).
24. Y. Shimizu *et al.* Nano-scale defect mapping on a magnetic disk surface using a contact sensor. *IEEE Trans. Magn.* **47,** 3426–3432 (2011).
25. K. Merchant, P. Mee, M. Smallen & S. Smith. Lubricant bonding and orientation on carbon coated media. *IEEE Trans. Magn.* **26,** 2688–2690 (1990).
26. Alejandro Rodriguez-Mendez & David B. Bogy. Lubricant flow and accumulation on the slider's air-bearing surface in a hard disk drive. *Tribol. Lett.* **53,** 469–476 (2014).
27. Yung-Kan Chen, Jinglin Zheng & David B Bogy. Light contact and surfing state dynamics of air bearing sliders in hard disk drives. *Appl. Phys. Lett.* **100,** (2012).
28. John Crank. *The mathematics of diffusion*. (Oxford university press, 1979).